# Raman Tensor Formalism for Optically Anisotropic Crystals

Christian Kranert,[*] Chris Sturm,[†] Rüdiger Schmidt-Grund, and Marius Grundmann

*Universität Leipzig, Institut für Experimentelle Physik II, Abteilung Halbleiterphysik, Linnéstraße 5, 04103 Leipzig, Germany*

We present a formalism for calculating the Raman scattering intensity dependent on the polarization configuration for optically anisotropic crystals. It can be applied to crystals of arbitrary orientation and crystal symmetry measured in normal incidence backscattering geometry. The classical Raman tensor formalism cannot be used for optically anisotropic materials due to birefringence causing the polarization within the crystal to be depth dependent. We show that in the limit of averaging over a sufficiently large scattering depth, the observed Raman intensities converge and can be described by an effective Raman tensor given here. Full agreement with experimental results for uniaxial and biaxial crystals is demonstrated.

The most basic equation of Raman scattering is that connecting the scattering intensity and scattering geometry by the Raman tensor. This relation is found in any textbook on Raman scattering, particularly also in those specific to crystalline materials [1,2]. Yet it has been known for almost 80 years that this relation cannot be applied to anisotropic materials due to birefringence [3,4]. This issue led to the conclusion that the analysis of intensities from Raman measurements of birefringent crystals with any polarization between the principal axes of the dielectric indicatrix is "pointless" [5]. In semiconductor research, this issue was not a problem for a long time since mainly opaque materials and/or materials with cubic symmetry have been investigated, for which the established formalism holds. However, more recently the investigation of typically anisotropic wide-band-gap semiconductors came into focus. Since the awareness for the problem faded over the years, the interpretation of the observed intensity dependence of the peaks in the Raman spectrum was attempted based on the classic Raman tensor formalism, which required the introduction of unphysical *ad hoc* parameters such as a phase shift between the Raman tensor elements [6–10] or an intensity offset [11–13]. Further, theoretical calculations showed an unsatisfactorily resolved discrepancy to experimental results [14]. These approaches neglecting birefringence may also have been motivated by the at-first-surprising fact that the intensity dependencies are reproducible at completely different setups, while birefringence causes the direction of polarization to vary along the penetration depth, which is a characteristic property of the focusing optics. This reproducibility could not be explained by a first approach to take the birefringence into account [15].

Here, we solve these issues by integration over the scattering depth range and considering the effect due to birefringence. As a result, we obtain a general formalism for the polarization dependence of the scattering intensity

in normal-incidence backscattering for any crystalline sample. It explains the correct physical origin and magnitude of the apparent phase shift and the loss of depth dependence as a consequence of a sufficiently large scattering depth.

In the following, we restrict our calculations to backscattering with normal incidence. This can also be considered to approximately hold for focusing optics with moderately wide apertures, depending on the refractive index of the sample. Further, we assume an excitation photon energy in the transparency regime that is much larger than the phonon energy such that incident and scattered photon energy can be assumed to be approximately equal. At first, we study the case for which one principal axis of the indicatrix is normal to the surface. The general case is discussed at the end of the text. Within this approximation, the polarization of the incident and scattered radiation is restricted to a plane perpendicular to the excited crystal surface; i.e., the problem becomes two dimensional. For scattering by phonons excited in the transparency regime, the Raman tensor is symmetric with real components [1,16]. Thus, in two dimensions it generally takes the form

$$\mathcal{R} = \begin{pmatrix} a & d \\ d & b \end{pmatrix}. \qquad (1)$$

The Raman intensity is determined from the Raman tensor by the relation [1,2,16]

$$I \propto |\boldsymbol{e}_1 \mathcal{R} \boldsymbol{e}_0|^2, \qquad (2)$$

where $\boldsymbol{e}_0$ and $\boldsymbol{e}_1$ are the electric field vectors of the incident and scattered radiation at the position of the scattering event. Owing to the birefringence, these are not necessarily identical to the polarizations of the incident and scattered radiation $\boldsymbol{e}_i$ and $\boldsymbol{e}_s$ accessible by experiment. We consider

the part of the sample above the scattering event as an optical element. Its effect on the polarization can be described applying a Jones matrix [17] $J(z)$, which depends on the thickness of the slab $z$. Since the scattered radiation has to pass back through the sample the same way as the incident radiation, Eq. (2) becomes

$$I \propto |e_s S(\theta) J(z) \mathcal{R} J(z) S^{-1}(\theta) e_i|^2 \qquad (3)$$

for the experimentally accessible light polarizations. The rotation matrix $S(\theta)$ transforms the system of allowed polarizations for the excited surface at the excitation wavelength into the laboratory system [17]. The absolute phase of the radiation is neglected because only intensities are measured in Raman experiments. Thus, the Jones matrix can be normalized to the first entry and, in the basis of allowed polarizations, takes the simple diagonal form [17]:

$$J(z) = \begin{pmatrix} 1 & 0 \\ 0 & e^{i\chi(z)} \end{pmatrix}. \qquad (4)$$

The phase shift $\chi(z)$ between light with polarization parallel to the fast and slow axis, with the difference in refractive indices $\Delta n$, is $\chi(z) = 2\pi\Delta n z/\lambda$. Since we neglect the difference of the wavelength $\lambda$ for incident and scattered light, $\chi(z)$ is identical in both Jones matrices. We note that the Raman tensor $\mathcal{R}$ in Eq. (3) is actually already an effective Raman tensor in the sense of Ref. [18], which, however, has the same properties (symmetric, real valued) as the molecular Raman polarizability tensor.

The form of Eq. (3) suggests that the term $\mathcal{R}_{\mathrm{eff}}(z) = S(\theta)J(z)\mathcal{R}J(z)S^{-1}(\theta)$ acts as a depth-dependent effective Raman tensor. Expanding this term yields an expression of the form

$$\mathcal{R}_{\mathrm{eff}}(z) = \mathcal{R}_0 + \mathcal{R}_1 e^{i\chi(z)} + \mathcal{R}_2 e^{i2\chi(z)}, \qquad (5)$$

with the explicit terms

$$\mathcal{R}_0 = a \begin{pmatrix} \cos^2(\theta) & \sin(\theta)\cos(\theta) \\ \sin(\theta)\cos(\theta) & \sin^2(\theta) \end{pmatrix}, \qquad (6a)$$

$$\mathcal{R}_1 = d \begin{pmatrix} -2\sin(\theta)\cos(\theta) & \cos^2(\theta) - \sin^2(\theta) \\ \cos^2(\theta) - \sin^2(\theta) & 2\sin(\theta)\cos(\theta) \end{pmatrix}, \qquad (6b)$$

$$\mathcal{R}_2 = b \begin{pmatrix} \sin^2(\theta) & -\sin(\theta)\cos(\theta) \\ -\sin(\theta)\cos(\theta) & \cos^2(\theta) \end{pmatrix}. \qquad (6c)$$

If the laboratory system is chosen equivalently to the system of allowed polarizations, i.e., $\theta = 0$, these simplify to

$$\mathcal{R}_0 = \begin{pmatrix} a & 0 \\ 0 & 0 \end{pmatrix}, \quad \mathcal{R}_1 = \begin{pmatrix} 0 & d \\ d & 0 \end{pmatrix}, \quad \mathcal{R}_2 = \begin{pmatrix} 0 & 0 \\ 0 & b \end{pmatrix}. \qquad (7)$$

In a Raman experiment, scattering by phonons is excited in and collected from a certain depth range within the crystal. Assuming a homogeneous intensity distribution in a sample ranging from $z_1$ to $z_2$, the apparent effective Raman tensor is obtained by integration:

$$\mathcal{R}_{\mathrm{eff}} = \frac{1}{\Delta z} \int_{z_1}^{z_2} \mathcal{R}_0 + \mathcal{R}_1 e^{i\chi(z)} + \mathcal{R}_2 e^{i2\chi(z)} dz. \qquad (8)$$

Obviously, in the limit of large $\Delta z = z_2 - z_1$, the integral corresponds to a Fourier transformation. Since $\chi$ is linear in $z$, the exponential functions and the constant coefficient 1 of $\mathcal{R}_0$ correspond to the base of the $L^2$ space. Thus, in this limit the three components $\mathcal{R}_0$, $\mathcal{R}_1$, and $\mathcal{R}_2$ are orthogonal to each other. This allows us to write the scattering intensity as

$$I \propto |e_s \mathcal{R}_0 e_i|^2 + |e_s \mathcal{R}_1 e_i|^2 + |e_s \mathcal{R}_2 e_i|^2. \qquad (9)$$

These three terms $e_s \mathcal{R}_k e_i$ are referred to as $\mathcal{E}_k$ in the following.

While Eq. (9) is strictly true only for an integration over an infinite scattering depth, it approximately holds also for sufficiently large $\Delta z$. In order to investigate the general case, we consider a finite integration. In this case, the intensity is neither $I = |\mathcal{E}_0 + \mathcal{E}_1 + \mathcal{E}_2|^2$ as according to Eq. (2) nor $I = |\mathcal{E}_0|^2 + |\mathcal{E}_1|^2 + |\mathcal{E}_2|^2$ according to Eq. (9), but something in between, depending on the integration range. This can be described using three vectors $x_k$ in three-dimensional space with length $\mathcal{E}_k$ which are oriented such that $I = |x_0 + x_1 + x_2|^2$. Since the convergence is slower considering a phase shift of $\chi$ instead of $2\chi$, we consider the planar problem including $x_0$ and $x_1$ with an apparent angle $\xi$ between both, such that $x_0 x_1 = \mathcal{E}_0 \mathcal{E}_1 \cos(\xi)$. The apparent angle $\xi'$ between the $x_0$ and $x_2$ components is calculated analogously and converges twice as fast. We further introduce the normalized function $f(z)$, which describes the scattering depth profile. The apparent angle is then calculated as

$$\xi = \arccos\left(\frac{\int_0^\infty f(z)|\mathcal{E}_0 + \mathcal{E}_1 e^{i\chi(z)}|^2 dz - \mathcal{E}_0^2 - \mathcal{E}_1^2}{2\mathcal{E}_0 \mathcal{E}_1}\right). \qquad (10)$$

The colinear case $\xi = 0$ corresponds to $I = |\mathcal{E}_0 + \mathcal{E}_1 + \mathcal{E}_2|^2$, and $\xi = \pi/2$ corresponds to $I = |\mathcal{E}_0|^2 + |\mathcal{E}_1|^2 + |\mathcal{E}_2|^2$.

For the measurement of sufficiently thick single crystals, the depth profile is given by the focusing optics, which can be approximated by a Gaussian depth profile function with broadening $\sigma$ corresponding to the depth resolution. The resulting apparent angle $\xi$ for focusing on the sample surface, i.e., with the Gaussian profile centered at 0, is depicted in Fig. 1(a). It converges quickly to $\pi/2$ and is
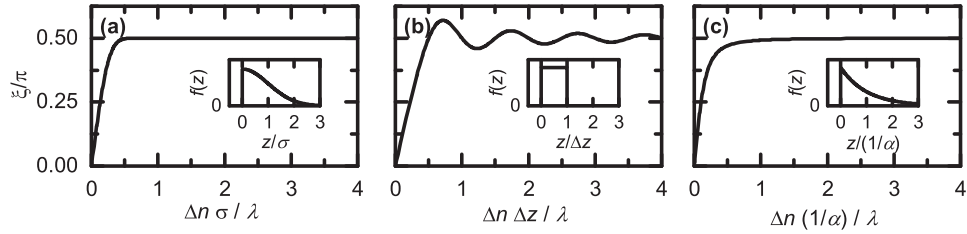
FIG. 1.  Dependence of the effective angle $\xi$ on (a) the width $\sigma$ of a Gaussian profile centered at the sample surface, (b) the slab thickness $\Delta z$ for a rectangular depth profile, and (c) the extinction coefficient $\alpha$ of an absorptionlike depth profile. The depth profile functions $f(z)$ are plotted in the respective insets. For $\lambda = 500$ nm and $\Delta n = 0.02$, a value of 1 on the abscissa corresponds to 25 $\mu$m for $\sigma$, $\Delta z$, or $1/\alpha$.

close to that already for $\sigma = 0.3\lambda/\Delta n$. Assuming a moderate birefringence of $\Delta n = 0.02$ and an excitation wavelength of $\lambda = 500$ nm, $\xi \approx \pi/2$ is already fulfilled for a depth resolution of 7 $\mu$m, a value typically exceeded in experimental setups for the investigation of bulk crystals, explaining identical results obtained with completely different setups. As a consequence, for the investigation of transparent bulk crystals, the experimental setup can typically be chosen such that the above given formulas hold in very good approximation, allowing us to calculate the scattering intensity from the polarization configuration.

The thickness of thin films is typically significantly smaller than the depth resolution; thus, a rectangular depth profile from 0 to $\Delta z$ is often a good approximation (reflections at the interfaces are neglected for simplicity). The integration yields the dependence depicted in Fig. 1(b), showing that values of $\Delta z$ and $\Delta n$ yielding $0 < \xi < \pi/2$ are not uncommon. In this case, the problem becomes three dimensional and can, in general, be solved by numeric integration. An alternative approach is described in the Supplemental Material [19].

For completeness, the calculation for a depth profile according to an absorption is given in Fig. 1(c). It converges similarly to the Gaussian profile, but slightly slower. We stress that the assumptions on the form of the Raman tensor and the Jones matrix made above are only valid in the absence of any resonances, which might not hold if absorption occurs. For strong absorption, as for direct semiconductors excited well above their band gap energy, the absorption is typically so strong that $\xi \approx 0$ and, therefore, $\boldsymbol{e}_0 = \boldsymbol{e}_i$ and $\boldsymbol{e}_1 = \boldsymbol{e}_s$ approximately hold.

In order to verify our considerations above, we carried out Raman measurements of uniaxial ZnO and biaxial $\beta$-Ga$_2$O$_3$. We used commercial samples by Crystec and Tamura, respectively, the latter having been confirmed to be single crystalline by x-ray studies (cf. Supplemental Material [19]). The polarization of incident and detected light was rotated by $\varphi$ relative to the crystal using a $\lambda/2$ wave plate while keeping the analyzer fixed. Both parallel $(\boldsymbol{e}_i \| \boldsymbol{e}_s)$ and cross-polarized $(\boldsymbol{e}_i \perp \boldsymbol{e}_s)$ configurations were used. From the spectra, we obtained the intensities for the individual phonon modes as the area of Lorentzian

functions used to model the line shape of the respective Raman lines. We used an excitation at $\lambda = 532$ nm with a microscope objective with a numerical aperture of NA = 0.42, which yields a depth resolution > 10 $\mu$m. Detailed information on the experimental procedure can be found in the Supplemental Material [19].

We first consider the simple and common case of a rectangular symmetry of the excited crystal face, i.e., an in-plane $mm2$ symmetry. This is, for example, the case for the $a$ or $m$ plane of hexagonal crystals like ZnO, which is shown in Fig. 2. In this case, several simplifications apply. The principle axes of the indicatrix can be identified with crystallographic axes. Consequently, the laboratory coordinate system can easily be set such that $\theta = 0$. Further, the two-dimensional Raman tensor for phonon modes and excitation on such a plane has either off-diagonal or diagonal elements only [1]. In the first case, $\mathcal{R}_0$ and $\mathcal{R}_2$ vanish and the effective Raman tensor $\mathcal{R}_{\text{eff}} = \mathcal{R}_1$ is identical to the unmodified one and independent from the scattering depth. In the latter case, only $\mathcal{R}_1$ vanishes and the scattering intensity is described by $\mathcal{R}_0$ and $\mathcal{R}_2$ from Eq. (7). The resulting angular dependence can be equivalently expressed using a single, complex matrix,

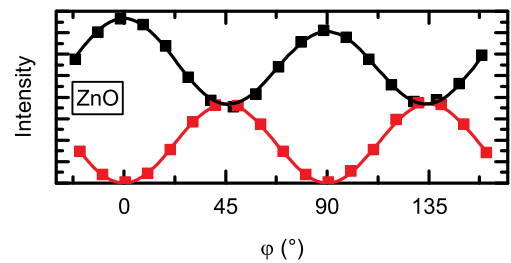$$\mathcal{R}_{\text{eff}} = \begin{pmatrix} a & 0 \\ 0 & be^{i\xi'} \end{pmatrix}, \tag{11}$$



FIG. 2.  Dependence of the Raman intensity of the $A_1$(TO) phonon mode of ZnO on the angle between the polarization and the $c$ axis for parallel polarization $(\boldsymbol{e}_i \| \boldsymbol{e}_s)$ (black) and cross polarization $(\boldsymbol{e}_i \perp \boldsymbol{e}_s)$ (red). The bottom axis corresponds to an intensity of 0. The experimental data (scatter plot) were fitted (solid line) using Eq. (9).

where $\xi'$ can be read off Fig. 1 using halved values for the abscissa. This explains the very good agreement obtained by several groups using such an approach to model the angular intensity dependence [6–8]. Actually, for these transparent materials, values around $\xi' \approx \pi/2$ were reported, indicating an integration over a sufficiently large scattering depth. Our experimental data for ZnO in Fig. 2 can also be modeled very well using $\xi' = \pi/2$. For materials excited in the absorption regime, complex Raman tensor elements might actually occur and have been reported [20,21]. However, depending on the magnitude of birefringence and the absorption coefficient [cf. Fig. 1(c)], a possible influence of the birefringence should be considered since it has a qualitatively similar effect.

In some reports, the angular polarization dependence was modeled using only real Raman tensor elements with opposite signs for $a$ and $b$ [11–13]. However, the applied formulas require that an empirical intensity offset must have been used. Using the Raman tensor formalism introduced here, these experimental data can be modeled well without any additional parameters, assuming $\xi' = \pi/2$. We note that the signs of the Raman tensor elements are not accessible by measurements on a single surface if $\xi' = \pi/2$.

Raman measurements of the $A_g$ modes of monoclinic $\beta$-Ga$_2$O$_3$ with excitation on its (0$\bar{1}$0) plane pose the most demanding test for the introduced formalism in its most general form due to the low symmetry of this surface. The optical parameters were determined by spectroscopic ellipsometry [22]: The birefringence on this surface is approximately $\Delta n = 0.027$ and $\theta = 3.8°$ if the coordinate system is set such that $y \| [100]$ and $z \| [010]$. Consequently, the approximation Eq. (9) is expected to hold.

We successfully modeled the observed Raman intensities dependent on $\varphi$ for all ten $A_g$ phonon modes of $\beta$-Ga$_2$O$_3$ using Eq. (9) with only the three real Raman tensor elements as free parameters [see, for example, Figs. 3(a) and 3(c)]. For comparison with the approach used for wurtzite materials [6–8] discussed above, we modeled the same intensity dependencies using nonsymmetric, complex Raman tensor elements, neglecting effects due to birefringence [see Figs. 3(b) and 3(d)]. This approach uses seven free parameters (four absolute values of the tensor elements and three relative phase shifts). While some of the phonon modes could also be modeled with reasonable agreement using complex Raman tensors, the agreement with the experimental data was significantly worse for other phonon modes as compared to using Eq. (9), particularly for such modes with non-negligible tensor element $d$.

If no principal axis is parallel to the propagation direction, a polarization component parallel to the propagation direction may also occur. In this case, the dielectric tensor of the material at the excitation wavelength must be known. From that, the two semiaxes of the intersection
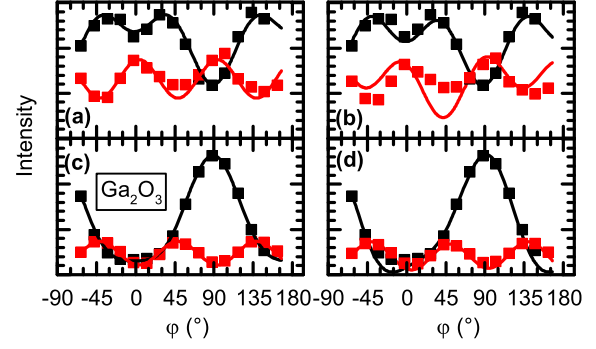


FIG. 3.   Same as Fig. 2 for two $A_g$ phonon modes of $\beta$-Ga$_2$O$_3$ excited on the (0$\bar{1}$0) plane. $\varphi = 0°$ corresponds to the direction of the $a$ axis. (a),(b) $A_g^{(4)}$ phonon at 320 cm$^{-1}$ and (c),(d) $A_g^{(10)}$ at 767 cm$^{-1}$. The experimental data (scatter plot) were fitted (solid line) (a),(c) using Eq. (9) and (b),(d) using a complex, non-symmetric Raman tensor.

ellipse between surface and indicatrix need to be determined. Let $z'$ be the direction of the surface normal. Then this approach yields the directions $x'$ and $y'$ of allowed displacement $\boldsymbol{D}_{1/2}$ in the crystal. We define the matrix $R$ as the transformation matrix from the system of principal axes to the system $x'$, $y'$, $z'$ set as the laboratory system; thus, $\theta = 0$. The definition of this system requires the components $\epsilon_{x'y'}$ of the transformed dielectric tensor $R\epsilon R^{-1}$ to be 0. Geometrical considerations further require either $\epsilon_{x'z'}$ or $\epsilon_{y'z'}$ to be 0 as well, depending on the choice of the axes $x'$ and $y'$. In the following, we choose the laboratory system such that $\epsilon_{xz} = 0$, without loss of generality. Using the coplanarity of $\boldsymbol{D}$, $\boldsymbol{E}$, and $\boldsymbol{k} \| z$ resulting from Maxwell's equations, the allowed electric field vectors can be calculated using $R\epsilon R^{-1}$ as $\boldsymbol{E}_1 = (1,0,0)^\top$ and $\boldsymbol{E}_2 = (\epsilon_{y'z'}^2 + \epsilon_{z'z'}^2)^{-1/2}(0, \epsilon_{z'z'}, \epsilon_{y'z'})^\top$. Applying the transformation matrix $T = (\boldsymbol{E}_1, \boldsymbol{E}_2)$, the experimentally accessible incident electric field can be transformed to that within the crystal. Therefore, Eq. (3) can be generalized to

$$I \propto |\boldsymbol{e}_s S(\theta) J(z') T^\top R\mathcal{R}R^{-1} T J(z') S^{-1}(\theta) \boldsymbol{e}_i|^2. \quad (12)$$

The effective Raman tensor $\mathcal{R}_{\text{eff}} = J(z') T^\top R\mathcal{R}R^{-1} T J(z')$ remains two dimensional and the deliberations above on the dependence on the slab thickness hold; i.e., the Raman tensor has the same form as in Eq. (5) and components similar to Eq. (7). Assuming that the tensor elements of the transformed, symmetric Raman tensor $R\mathcal{R}R^{-1}$ are labeled $r_{x'y'}$ for the $xy$ and $yx$ components, and so on, the tensor elements of Eq. (7) must be replaced as follows:

$$a = r_{x'x'}, \quad (13a)$$

$$b = \frac{r_{y'y'}\epsilon_{z'z'}^2 + 2r_{y'z'}\epsilon_{y'z'}\epsilon_{z'z'} + r_{z'z'}\epsilon_{y'z'}^2}{\epsilon_{y'z'}^2 + \epsilon_{z'z'}^2}, \quad (13b)$$

$$d = \frac{r_{x'y'}\epsilon_{z'z'} + r_{y'z'}\epsilon_{y'z'}}{\sqrt{(\epsilon_{y'z'}^2 + \epsilon_{z'z'}^2)}} . \qquad (13c)$$

If $z'$ is parallel to a principal axis, the off-diagonal element $\epsilon_{y'z'}$ vanishes and the simplified form is restored. We note that generally the off-diagonal elements are at least 1 order of magnitude smaller than the diagonal elements. Thus, Eq. (13) is only a small correction. For all samples investigated by us, this correction was smaller than the experimental uncertainty.

In summary, we have introduced a formalism that allows us to model the Raman scattering intensity for any polarization configuration in normal incidence backscattering for optically anisotropic crystals. A simple, depth-independent effective Raman tensor formalism can be used for an integration over a sufficiently large scattering depth, which is most often the case for measurements of transparent single crystals, but not for thin films or in the absorption regime. While the birefringence can be neglected for strong absorption, its effect on thin film measurements depends on the film thickness and the magnitude of the birefringence.

———————————

[*]christian.kranert@uni-leipzig.de

[†]csturm@uni-leipzig.de

[1] W. Hayes and R. Loudon, *Scattering of Light by Crystals*, 1st ed. (Dover Publications, New York, 2004).

[2] P. Y. Yu and M. Cardona, *Fundamentals of Semiconductors: Physics and Materials Properties* (Springer, New York, 1996).

[3] H. Michalke, Z. Physik. **108**, 748 (1938).

[4] S. P. S. Porto, J. A. Giordmaine, and T. C. Damen, Phys. Rev. **147**, 608 (1966).

[5] I. R. Beattie and T. R. Gilson, Proc. R. Soc. A **307**, 407 (1968).

[6] H. C. Lin, Z. C. Feng, M. S. Chen, Z. X. Shen, I. T. Ferguson, and W. Lu, J. Appl. Phys. **105**, 036102 (2009).

[7] T. Sander, S. Eisermann, B. K. Meyer, and P. J. Klar, Phys. Rev. B **85**, 165208 (2012).

[8] W. Zheng, R. S. Zheng, H. L. Wu, and F. D. Li, J. Alloys Compd. **584**, 374 (2014).

[9] N. Djiedeu, B. Mohamadou, P. Bourson, and M. Aillerie, J. Phys. Condens. Matter **21**, 015905 (2009).

[10] N. Djiedeu, B. Mohamadou, R. M. Erasmus, P. Bourson, and M. Aillerie, Int. J. Mod. Phys. Appl. **2**, 19 (2015).

[11] G. Pezzotti, H. Sueoka, A. A. Porporati, M. Manghnani, and W. Zhu, J. Appl. Phys. **110**, 013527 (2011).

[12] M. C. Munisso, W. Zhu, and G. Pezzotti, Phys. Status Solidi B **246**, 1893 (2009).

[13] M. Deluca, M. Higashino, and G. Pezzotti, Appl. Phys. Lett. **91**, 091906 (2007).

[14] A. Calzolari and M. B. Nardelli, Sci. Rep. **3**, 2999 (2013).

[15] P. Alonso-Gutiérrez, M. L. Sanjuán, and M. C. Morón, Phys. Rev. B **71**, 085205 (2005).

[16] G. Placzek, in *Handbuch der Radiologie, Band VI, Teil II*, edited by E. Marx (Akademische Verlagsgesellschaft, Leipzig, 1934).

[17] R. C. Jones, J. Opt. Soc. Am. **31**, 488 (1941).

[18] M. Gorkunov and M. Ryazanov, J. Exp. Theor. Phys. **85**, 97 (1997).

[19] See Supplemental Material at http://link.aps.org/supplemental/10.1103/PhysRevLett.116.127401 for a detailed description of the experimental procedure, an approach to model the Raman intensities in the non-convergent case and x-ray data of one of the $Ga_2O_3$ single crystals.

[20] T. Strach, J. Brunen, B. Lederle, J. Zegenhagen, and M. Cardona, Phys. Rev. B **57**, 1292 (1998).

[21] H. B. Ribeiro, M. A. Pimenta, C. J. S. de Matos, R. L. Moreira, A. S. Rodin, J. D. Zapata, E. A. T. de Souza, and A. H. Castro Neto, ACS Nano **9**, 4270 (2015).

[22] C. Sturm, J. Furthmüller, F. Bechstedt, R. Schmidt-Grund, and M. Grundmann, APL Mater. **3**, 106106 (2015).